Faraday Discuss., 1997, **108**, 101–113

Time-resolved studies of dynamics in molecular and cluster anions

B. Jefferys Greenblatt, Martin T. Zanni and Daniel M. Neumark*

Department of Chemistry, University of California, Berkeley, CA 94720, USA and Chemical Sciences Division, Lawrence Berkeley National Laboratory, Berkeley, CA, USA

Femtosecond photoelectron spectroscopy (FPES) is used to study the time-resolved photodissociation dynamics of $I_2^-(CO_2)_{n=4,16}$ clusters excited at 780 nm. The FPES experiment on $I_2^-(CO_2)_4$ shows that the I^- fragment formed by excitation to the $A'\,^2\Pi_{1/2,g}$ repulsive state of I_2^- initially pulls away from the cluster, but by 0.2 ps it is drawn back to complex with more of the solvent molecules. In the $n = 16$ cluster, where caging of the I_2^- is known to be complete, FPES probes the recombination dynamics of the I_2^- in considerable detail. Specifically, vibrational relaxation on the I_2^- $X\,^2\Sigma_u^+$ state and the accompanying evaporation on CO_2 molecules can be followed in real time. Vibrational relaxation is essentially complete by 10 ps, whereas solvent evaporation is not entirely complete by 200 ps. The spectra also show evidence for short-lived recombination on the I_2^- $A\,^2\Pi_{3/2,g}$ state. The results are compared to previous experimental results for $I_2^-(Ar)_n$ clusters and recent simulations of cluster dynamics.

Introduction

The effect of clustering on the dynamics of elementary chemical processes has been the focus of considerable interest, as it offers a route toward understanding the evolution of chemistry from gas phase to condensed phase environments. Much of the original work in this area focused on neutral van der Waals clusters,[1–3] in which a chromophore such as I_2 was complexed to one or more solvating species, and the resulting effects on the chromophore photophysics were probed using laser-induced fluorescence, multiphoton ionization, and other spectroscopic/dynamical probes. More recently, femtosecond time-resolved techniques have been applied to clusters of this type.[4,5] A parallel effort has developed in the study of ionic clusters comprised of solvated charged chromophores.[6] These experiments have an advantage over neutral cluster studies in that there is generally no ambiguity concerning the size of the cluster, an important issue if one is trying to probe size-dependent effects. Clusters of I_2^- with Ar and CO_2 have been of particular recent interest; the photodissociation dynamics of these clusters have been studied in an elegant series of frequency and time-resolved experiments by Lineberger and co-workers.[7–14] We have undertaken studies of these clusters using a new experimental technique, femtosecond photoelectron spectroscopy (FPES), providing a picture of the photodissociation dynamics that in many ways complements the Lineberger experiments. Previously we have reported results on I_2^- and $I_2^-(Ar)_n$ clusters.[15,16] Here new results for $I_2^-(CO_2)_n$ clusters are presented and discussed in light of earlier experiments on $I_2^-(Ar)_n$ clusters.

Two types of experiments have been performed by Lineberger's group on clusters of I_2^- and other dihalides with CO_2 and Ar. In the experiments on I_2^- (see Fig. 1) the anion is photoexcited from the $X\,^2\Sigma_u^+$ state to a repulsive electronic state, the $A'\,^2\Pi_{1/2,g}$ state, and the subsequent interactions between the recoiling photofragments and solvent

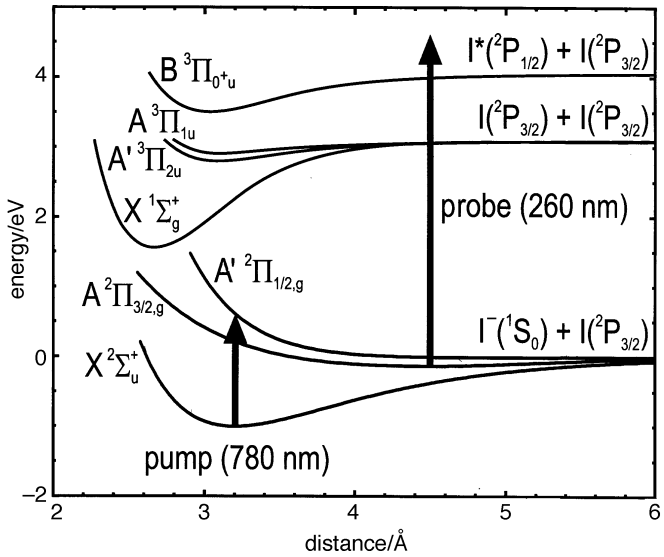

Fig. 1 Potential energy curves for low-lying electronic states of I_2^- and I_2. Correlating atomic states are indicated to the right. The anion $X^2\Sigma_u^+$ and $A\,^2\Pi_{3/2,g}$ state parameters are taken from ref. 16. The anion $A'\,^2\Pi_{1/2,g}$ state parameters are taken from ref. 37. Neutral state parameters are from ref. 38–41.

species (S) are probed. In one set of experiments[7,8,13,17] the product masses from one-photon dissociation were determined. These experiments show that for small numbers of solvent species only 'uncaged' ionic products of the type $I^-(S)_n$ are produced, whereas for larger clusters stable products of the type $X_2^-(S)_n$ dominate. These 'caged' products result from recombination of the photofragments on a lower-lying, bound state of I_2^-, a process analogous to geminate recombination in solution.[18] The second set of experiments[9–11,14] used a two-photon pump-and-probe scheme with picosecond and, more recently, femtosecond lasers to perform time-resolved studies of the recombination dynamics in clusters of I_2^- sufficiently large so that caging occurs. In these experiments the I_2^- chromophore is dissociated with the pump pulse, and subsequent absorption of the probe pulse (of the same color) is monitored as a function of delay time. The experiments yield the overall time-scale for recombination and vibrational relaxation of the I_2^- on its ground electronic state: 1.3 ps in the case of $I_2^-(CO_2)_{16}$, *vs.* 130 ps for $I_2^-(Ar)_{20}$.[14] While the recovery of the I_2^- absorption is monotonic for $I_2^-(Ar)_n$ clusters, the results for $I_2^-(CO_2)_{16}$ have been interpreted in terms of 'coherent recombination' of the photofragments occurring on the $A\,^2\Pi_{3/2,g}$ excited state of I_2^- (see Fig. 1) *ca.* 2 ps after the pump pulse.[9,10,14] In related work, the time-resolved recombination dynamics of I_2^- in solution were studied by Barbara and co-workers *via* transient absorption in a variety of polar solvents.[19,20] The absorption recovery times lie in the range of a few picoseconds, *i.e.* a similar time-scale to the $I_2^-(CO_2)_n$ clusters.

The finite clusters have been considered in a series of theoretical papers in which molecular dynamics simulations are used to determine the equilibrium geometries of the clusters and track the dynamics subsequent to photodissociation of the dihalide chromophore. The original studies by Perera and Amar[21] focused on the time-scales for recombination and solvent evaporation on the ground electronic state of the dihalide. More recent work by Batista and Coker[22] and Parson and co-workers[23–25] has considered the importance and time-scale of non-adiabatic electronic transitions that occur subsequent to photoexcitation. Parson in particular has emphasized the role of 'anomalous charge switching' in these clusters, in which the asymmetric charge distribu-

tion on the two iodine atoms induced by solvation in the cluster ground state is reversed in the photoexcited state.

The FPES experiments discussed here were undertaken to provide a more complete picture of the dissociation dynamics in $I_2^-(CO_2)_n$ clusters. In these experiments, the I_2^- chromophore is excited to the repulsive $A'\,^2\Pi_{1/2,g}$ state by an ultrafast (*ca.* 80 fs) pump pulse. The time-evolution of the cluster is monitored by photodetachment with an ultrafast probe pulse and measurement of the resulting photoelectron spectrum. At each pump–probe delay the photoelectron spectrum provides a 'snapshot' of the cluster dynamics, and is particularly sensitive to the local environment of the excess electron in the cluster. In contrast to Lineberger's pump–probe experiments, FPES can be used to investigate clusters in which no caging and recombination occurs. When recombination does occur, FPES can reveal the electronic state of the dihalide at each delay time, along with the degree of vibrational excitation and the approximate number of solvent species remaining in the cluster. Results are reported here for two clusters: $I_2^-(CO_2)_4$, for which almost no caging occurs, and $I_2^-(CO_2)_{16}$, in which caging is complete.

Experimental

Although the FPES experiment has been described in detail elsewhere,[15] several improvements have been made recently and are discussed below. Fig. 2 shows the apparatus. Cluster anions are generated by passing a mixture of 3% CO_2 in Ar over I_2 crystals at a backing pressure of 10–30 psig, expanding the gas mixture into a vacuum chamber through a piezoelectric valve running at a repetition rate of 500 Hz, and crossing the resulting free jet with a 1.5 keV electron beam just downstream of the nozzle. The resulting plasma cools collisionally to produce both positive and negative ions. After passing through a 5 mm diameter skimmer located 11 mm below the valve orifice, the negative ions are injected into a Wiley–McLaren time-of-flight mass spectrometer[26] by applying pulsed extraction and acceleration fields perpendicular to the beam axis. The final beam energy varies between 800 eV and 1.7 keV, depending on the voltages used. A three-plate pulsed mass gate[27] ensures that only anions of the desired mass interact with the lasers.

The original source chamber of our apparatus has been divided into two regions to accommodate additional differential pumping. Each region is now pumped by a Varian VHS-10 diffusion pump with 4400 l s^{-1} pumping speed; this results in a considerably lower pressure in the region where the ion extraction pulses are applied. On their way to the laser interaction region, the anions pass through two additional differentially pumped regions. The first differential region is pumped by a Varian VHS-6 diffusion

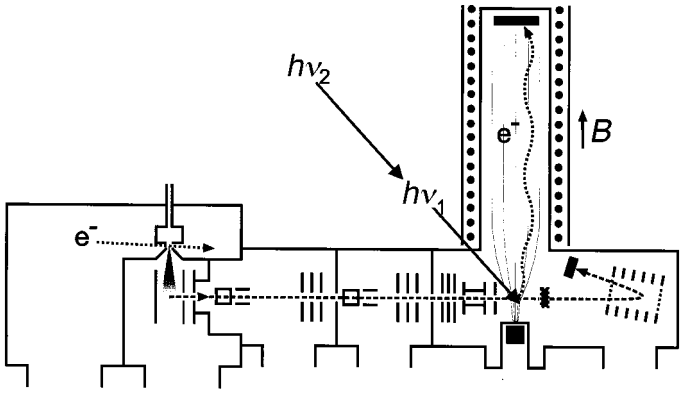

Fig. 2 Schematic diagram of the apparatus. Shown are the ion source, time-of-flight mass spectrometer, 'magnetic bottle' photoelectron spectrometer and reflectron photofragment analyzer.

pump. The second differential region and laser interaction region are each pumped by Varian V250 turbomolecular pumps. The base pressure in the final region is 1×10^{-9} Torr.

Laser pulses cross the ion beam at the focus of a 'magnetic bottle' photoelectron spectrometer, which is based on the design of Cheshnovsky *et al.*[27] However, a strong (0.8 T) permanent magnet, rather than an electromagnet, is used to produce the inhomogeneous magnetic field. It is located 9.5 mm below the beam axis, outside the vacuum chamber, and can be easily removed. A 1.3 m long solenoid field (20 G) guides the photoelectrons toward a 75 mm diameter dual microchannel plate detector. The arrival time distribution is recorded after each laser shot with a Stanford Research Systems SR430 multichannel scalar. Because of the inherently low resolution (*ca.* 250 meV) of a spectrometer which collects all of the electrons ejected from a fast-moving ion beam, a pulsed deceleration field is used to slow the ions down just before the interaction region.[28,29] This results in an improvement in the electron energy resolution of up to a factor of four, with further improvements expected shortly.

An in-line microchannel plate detector mounted on a retractable translator arm is used to record time-of-flight mass spectra of the ion beam. We can also measure the photofragment mass spectra resulting from excitation of a particular cluster with the pump pulse alone. To do this, the primary ion detector is retracted, allowing the ions to continue into an off-axis reflectron[7] which separates the daughter and parent ions. These are collected by another microchannel plate detector for photofragment mass analysis. Both types of mass spectra are recorded using a Tektronix TDS744A digitizing oscilloscope at a repetition rate of *ca.* 80 Hz.

The pump and probe laser pulses are generated from a commercial femtosecond laser system. A Coherent Innova-90 Ar^+ laser pumps a Clark-MXR NJA-5 Ti : sapphire oscillator. Selected pulses are amplified using a Clark-MXR regenerative amplifier system that includes a pulse stretcher, a Ti : sapphire regenerative amplifier pumped by a Nd : YAG laser running at a repetition rate of 500 Hz, and a pulse compressor. At 780 nm, the pump pulse wavelength, the pulse width and energy are 70 fs FWHM ($sech^2$) and 1 mJ, respectively. About 80% of this beam is directed into a frequency tripling unit (CSK Optronics 8315A), resulting in a probe pulse at 260 nm with width and energy of 110 fs and 20 μJ, respectively. (The width of the probe pulse is measured by difference frequency cross-correlation using a 300 μm thick KDP crystal.) The remainder of the 780 nm pulse passes through a computer-controlled variable delay line, and is then collinearly recombined with the probe pulse prior to entering the vacuum chamber. The polarization of the pump and probe pulses is perpendicular to the ion beam axis. For accurate determination of the temporal overlap of the pulses inside the vacuum chamber, two-color above threshold photodetachment (ATD) of I^- is used.[30]

Because the probe pulse wavelength is sufficient to detach electrons from ground state $I_2^-(Ar)_n$ and $I_2^-(CO_2)_n$ clusters, the photoelectron spectra are not background-free. Background subtraction is accomplished by either alternating 20 s scans between the desired delay and a fixed, negative (-2 ps) delay, or by using an optical chopper (New Focus 3501). The chopper blocks the pump pulse every other laser shot, and the SR430 scalar performs shot-by-shot background subtraction. Background spectra are also collected concurrently at 80 Hz repetition rate with the TDS744A oscilloscope. These are stored and used for longer-time normalization of the spectra. Depletion of the I_2^- ground state[31] causes a bleach of the background-subtracted signal, which is compensated by adding a percentage of the background back to the spectra.

Results

Fig. 3 shows FPES spectra of bare I_2^- for several pump–probe delay times. These spectra are taken using pulsed deceleration to slow down the ion beam; consequently

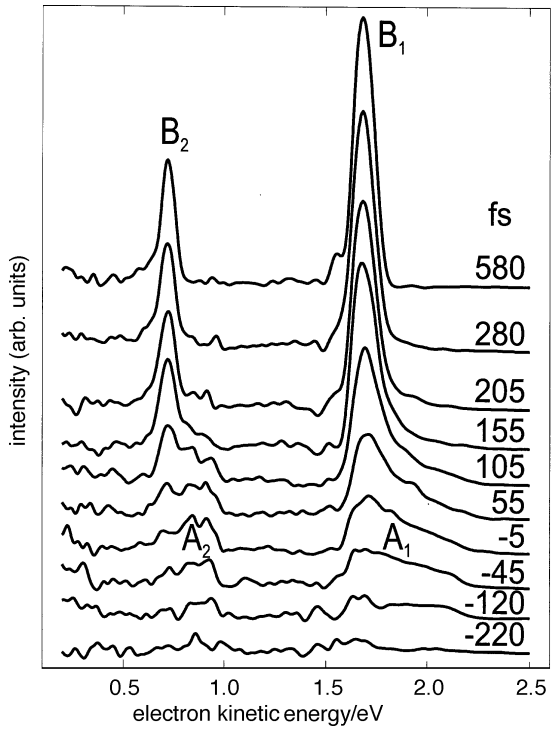

Fig. 3 Femtosecond photoelectron spectra of bare I_2^-, with decelerated ion beam. The pump–probe delay times are indicated to the right of the spectra. Assignments of various features are indicated, and explained in the text.

the electron energy resolution (*ca.* 100 meV) is substantially better than in our spectra reported and discussed previously.[15] As the delay time increases, two broad features, A_1 and A_2, shift toward lower electron energy and evolve into two sharp features, B_1 and B_2, at electron energies of 1.71 and 0.77 eV, respectively. Peaks B_1 and B_2 represent photodetachment of the I^- photoproduct to the $^2P_{3/2}$ and $^2P_{1/2}$ states of atomic iodine, respectively, whereas the broader features A_1 and A_2 at early times result from photodetachment of the dissociating wavepacket on the $A'\,^2\Pi_{1/2,g}$ anion state to the close lying $A'\,^3\Pi_{2u}$ and $A\,^3\Pi_{1u}$ states (A_1), and the $B\,^3\Pi_{0^+u}$ state (A_2) of neutral I_2. No evolution of the spectra occurs after 200 fs, indicating that dissociation of the bare ion is complete by this time.

Femtosecond photoelectron spectra for $I_2^-(CO_2)_4$ are shown in Fig. 4, also with a decelerated ion beam. At short times, from 0.0 to 0.1 ps, the evolution of the photoelectron signal between 1.4 and 2.0 eV is similar to bare I_2^-, in that a broad feature (A) arises and shifts toward lower electron energy to form a narrower peak (B_1). At lower energy, a second sharp feature (B_2) arises on the same time-scale. B_1 and B_2 are separated approximately by the spin–orbit splitting in atomic iodine (0.943 eV), and therefore appear to be analogous to the atomic I^- transitions in Fig. 3, although they are noticeably broader and shifted toward lower electron energy by 0.3 eV. By 0.2 ps, two new features are evident in the spectrum on the low energy side of B_1 and B_2, labelled C_1 and C_2, with each of the new features occurring at 0.14 eV lower electron energy than the main peaks. By 0.5 ps, each doublet has evolved into a single broad peak (D_1 and D_2). D_1 broadens and shifts toward lower electron energy from 0.3 to 2 ps, followed by a slight shift (0.05 eV) of the entire feature to higher energy between 2 and 200 ps.

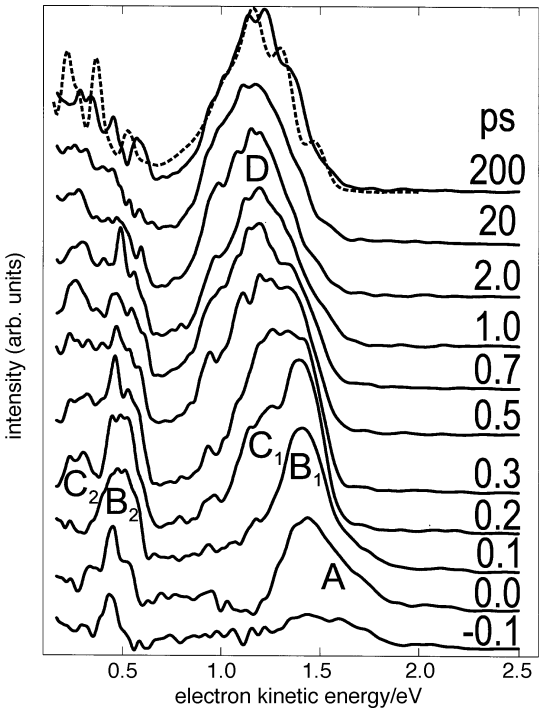

Fig. 4 Femtosecond photoelectron spectra of $I_2^-(CO_2)_4$ (with decelerated ion beam). A simulation (– – –) of the 200 ps spectrum is shown superimposed on the experimental spectrum. Labelled features are discussed in the next. Mass distribution used in simulation: $n = 1$, 23%; $n = 2$, 39%; $n = 3$, 30%; $n = 4$, 8%.

Fig. 5 shows femtosecond photoelectron spectra for $I_2^-(CO_2)_{16}$. In contrast to the I_2^- and $I_2^-(CO_2)_4$ spectra, no transitions to neutral electronic states correlating to $I(^2P_{1/2})$ are seen; these are too high in energy for the probe pulse because of stabilization energy of the anion from the 16 solvent molecules initially. At 0.0 ps, the spectrum consists of a broad, symmetric feature (A) centered at 0.72 eV, which is analogous to the transient in the FPES of bare I_2^-. As the delay time increases, this feature rapidly disappears, while another broad feature (B) centered at 0.38 eV dominates the spectrum by 0.2–0.4 ps. By 0.7 ps, this feature appears as a shoulder on a lower energy feature, labelled C in Fig. 5; this shoulder steadily decreases in intensity and disappears by 4.0 ps. An additional high energy feature (D) is apparent starting at 0.7 ps between 0.5 and 1.7 eV. This feature increases in intensity to 1.6 ps, and from 1.6 to 10 ps shifts gradually toward lower electron energy. During this time, feature C shifts toward higher energy, coalescing with D into a single feature (E) by 10 ps.

Discussion

$I_2^-(CO_2)_4$

It is instructive to compare the FPES results for $I_2^-(CO_2)_4$ with those obtained for $I_2^-(Ar)_6$.[16] Lineberger and co-workers found that $I^-(CO_2)_2$ and $I^-(Ar)$ are the dominant products from the photodissociation of $I_2^-(CO_2)_4$ at 720 nm and $I_2^-(Ar)_6$ at 790 nm, respectively.[8,13] At 780 nm, we measure essentially the same distribution of products for $I_2^-(CO_2)_4$ using the reflectron mass analyzer to separate the photoproducts from the pump laser alone. In spite of similar asymptotic product distributions for the

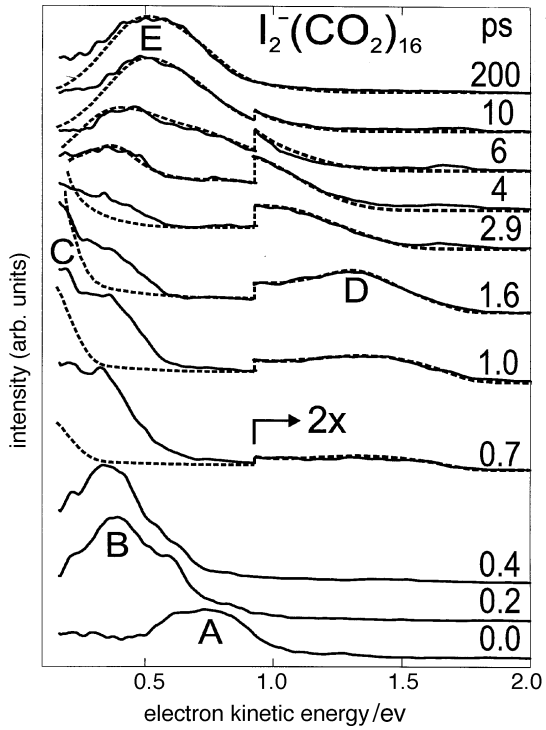

Fig. 5 $I_2^-(CO_2)_{16}$ femtosecond photoelectron spectra. Simulations (– – –) of spectra at 0.4 ps and later based on parameters in Table 1 are shown superimposed on experimental spectra. Between 0.7 and 10 ps, the vertical scale is expanded for energies larger than 0.9 eV. Labelled features are discussed in the text.

two anions, with essentially zero caging in both cases, the FPES spectra of $I_2^-(CO_2)_4$ differ significantly from those for $I_2^-(Ar)_6$. The $I_2^-(Ar)_6$ spectra show that the I_2^- bond breaks in approximately 200 fs, just as in bare I_2^-. The resulting 'I^-' features then shift toward higher electron energy from 240 to 1200 fs without otherwise changing in appearance, and do not evolve further after 1200 fs. This is due to a progressive weakening of the interaction between the I^- anion and the Ar solvent atoms as the charged photofragment leaves the cluster.[24]

In the $I_2^-(CO_2)_4$ spectra in Fig. 4, the narrow 'I^-' features, B_1 and B_2, are clearly apparent at 0.1 ps. They are shifted by 0.30 eV toward lower electron energy from bare I^-; this 'solvent shift' corresponds to 1.5 CO_2 molecules.[32] However, the appearance by 0.2 ps of features C_1 and C_2 at lower electron energy indicates that the interaction between the I^- fragment and solvent molecules has increased between 0.1 and 0.2 ps, and the subsequent evolution of the doublets into the broad features D_1 and D_2 by 0.5 ps implies that this interaction strengthens further during this time. The spectra thus suggest that the I^- fragment does not monotonically move away from the solvent species, as was the case in $I_2^-(Ar)_6$. Instead, it appears to initially pull away from the cluster (0.1 ps) but then complexes with the solvent molecules (0.2–0.5 ps). These dynamics are consistent with the considerably deeper well in $I^-\cdots CO_2$ (212 meV)[33] as compared to $I^-\cdots Ar$ (46 meV).[34] Fig. 6 shows a 'cartoon' of the dissociation dynamics.

Parson and co-workers have performed molecular dynamics simulations on somewhat larger $I_2^-(CO_2)_n$ clusters which show effects similar to those implied by our spectra.[25] These calculations show that in the X state of the cluster there is an asymmetric charge distribution on the two I atoms; the CO_2 molecules preferentially solvate

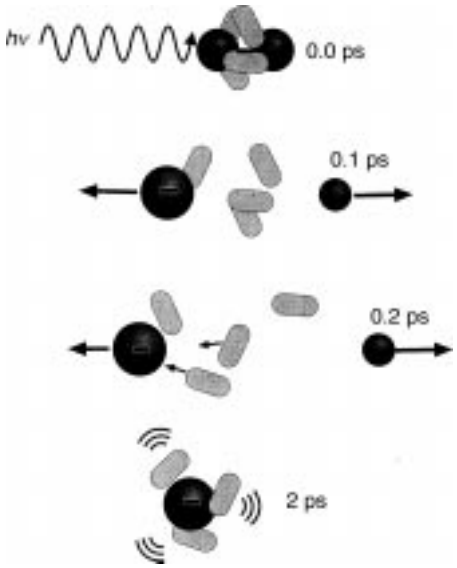

Fig. 6 'Cartoon' of dissociation dynamics in the $I_2^-(CO_2)_4$ cluster. Dark spheres indicate iodine atoms, and light elongated structures denote CO_2 molecules. The symbols ((( ))) indicate vibrational excitation.

the I atom with the larger negative charge. The situation is reversed upon excitation to the A′ state, an effect referred to as 'anomalous charge switching'.[24] Consequently, once dissociation begins, the I^- fragment is relatively unencumbered by solvent molecules. Although the interiodine distance rapidly increases, the attractive force between the I^- and the CO_2 molecules surrounding the I atom fragment is sufficient to prevent or at least slow down dissociation on the A′ state, and this attractive force results in the solvent atoms being drawn toward the I^-. The resulting more symmetric distribution of solvent molecules induces non-adiabatic transitions to the lower-lying A or X state. This is accompanied by rapid, asymmetric solvation of the I^-, leaving the neutral I fragment with its much weaker solvent interaction free to leave the cluster. These calculations therefore suggest that the rapid complexation of the I^- fragment and dissociation of the cluster as evidenced by the evolution of the sharp features B_1 and B_2 into the broader features D_1 and D_2 is associated at least in part with a non-adiabatic transition to one of the two lower-lying electronic states of the cluster.

Little change in the spectra occurs after 2 ps, so these photoelectron spectra are attributed to $I^-(CO_2)_n$ clusters. In this time regime, the number of CO_2 molecules solvated to the I^- fragment can be estimated by fitting the spectra to a distribution of $I^-(CO_2)_n$ photoelectron spectra; these spectra have been measured previously[32] and show that, for $n \leqslant 9$, each CO_2 molecule increases the electron binding energy by *ca.* 150 meV. The results of the best fit at 200 ps are shown superimposed on the experimental spectrum in Fig. 4; the assumed distribution is given in the caption. Note that the $n = 2$ and 3 clusters constitute the bulk of the products at 200 ps, with $n = 2$ being slightly dominant. This disagrees with the experimental mass distribution, in which $I^-(CO_2)_2$ and $I_2^-(CO_2)_3$ comprise 75% and 7% of the products, respectively.[35] This discrepancy may indicate that the time required to evaporate the last CO_2 molecule is longer than the time window of the experiments (200 ps), in contrast to the $I_2^-(Ar)_6$ results in which photoelectron spectra corresponding to the asymptotic ArI^- product were evident by 1.2 ps.[16] This explanation could be tested by measuring spectra at much larger (*ca.* ns)

delay times, which is feasible with a slight modification to the apparatus. We note that the $I^-(CO_2)_n$ spectra used to fit the spectrum in Fig. 4 were taken for cold anions; the imperfect fit at 200 ps may be an indication that this spectrum is from vibrationally excited $I^-(CO_2)_n$, a necessary condition for further evaporation.

$I_2^-(CO_2)_{16}$

Previous work on $I_2^-(CO_2)_{16}$ photodissociation at 720 nm and 790 nm by Lineberger and co-workers[8,9,35] shows 100% caging of the I_2^- product, with 7 (720 nm) or 6.5 (790 nm) CO_2 molecules lost, on average, *via* evaporative cooling as the I_2^- recombines and vibrationally relaxes. Time-resolved experiments[9,10,14] show that relaxation of the I_2^- is complete on a time-scale of several picoseconds, with the exact value depending on the photodissociation wavelength. Similar experiments on $I_2^-(Ar)_{20}$ also show 100% caging, but the product mass distribution is bimodal, split approximately evenly between bare I_2^- and $I_2^-(Ar)_{\langle n\rangle=11}$.[13,35] The I_2^- channel is attributed to recombination on the X state of I_2^-, and the FPES study of $I_2^-(Ar)_{20}$ shows that the other channel is due to recombination on the I_2^- A state; this state apparently survives for at least several microseconds, the time-scale of the Lineberger experiments. The FPES experiments on $I_2^-(Ar)_{20}$ also show that the time-scales for vibrational energy relaxation on the A and X states of I_2^- are 35 and 200 ps, respectively. The role of the A state in the dynamics of $I_2^-(CO_2)_{16}$ clusters following photoexcitation appears to be quite different. From the product mass distributions, it is clear that there is no asymptotic trapping on the A state. On the other hand, the time-resolved measurements by Lineberger show evidence for 'coherent recombination' on the A state at pump–probe delays around 2 ps.

With this background, we now consider the interpretation of the $I_2^-(CO_2)_{16}$ spectra in Fig. 5. There are several trends in these spectra to be understood: (1) the evolution and eventual disappearance of feature B from 0.2 to 4 ps; (2) the appearance of features C and D starting at 0.7 ps; and (3) the eventual coalescence of these two features by 10 ps. The second and third trends are similar to effects seen in the FPES of $I_2^-(Ar)_{20}$ and are attributed to vibrational relaxation of the I_2^- chromophore on the X state potential energy curve. As shown in Fig. 7, photodetachment from a highly vibrationally excited anion state results in well separated high and low energy features in the photoelectron spectrum corresponding to transitions from the inner and outer turning points, respectively, of the vibrational wavefunction on the I_2^- $X\,^2\Sigma_u^+$ state to the $X\,^1\Sigma_g^+$ state of neutral I_2. As the I_2^- vibrationally relaxes, the inner and outer turning points coalesce, as will the two corresponding features in the photoelectron spectrum. Hence, the first appearance of the high energy feature D indicates that recombination on the X state has occurred by 0.7 ps, resulting in highly excited I_2^-. The subsequent coalescence of features C and D by 10 ps represents the time-scale over which vibrational relaxation is complete. We note that a full coalescence of the analogous features in the $I_2^-(Ar)_{20}$ FPES does not occur, because all of the Ar atoms evaporate before the I_2^- relaxes to its vibrational ground state. In $I_2^-(CO_2)_{16}$, the evaporation of each CO_2 molecule removes considerably more energy from the cluster (*ca.* 240 *vs.* 73 meV),[13,35] so I_2^- can easily relax to its ground vibrational state without evaporation of all the solvent molecules.

This process of vibrational relaxation and solvent evaporation can be treated more quantitatively by simulating the FPES at various delay times in order to determine the average level of vibrational excitation and the number of solvent molecules remaining on the cluster as a function of time. To do this one needs to know how much each CO_2 molecule increases the electron binding energy of the I_2^-. We have measured photoelectron spectra of several $I_2^-(CO_2)_n$ clusters using the probe laser alone, and find an average increase of 80 meV per CO_2 molecule [significantly less than the 140 meV shift for $I^-(CO_2)_n$]. Assuming this to be independent of the I_2^- vibrational state, the simulations in Fig. 5 can be generated using a range of vibrational levels and cluster sizes, the

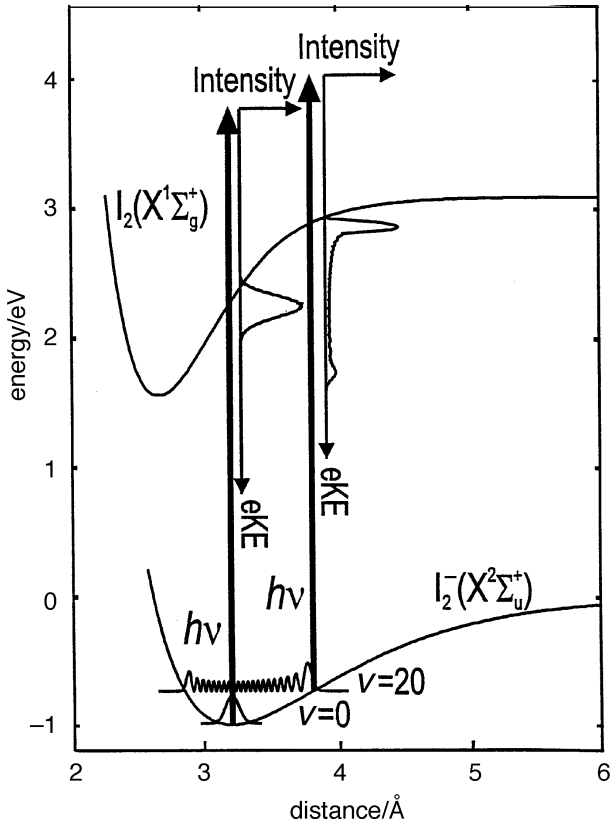

Fig. 7 Simulated I_2^- $X\,^2\Sigma_u^+$ state $v = 0$ and $v = 20$ vibrational wavefunctions, and photoelectron spectra

average values of which are given in Table 1. Thus, for example, at 1.6 ps, the simulations assume a broad vibrational level distribution ($16 \leqslant v \leqslant 55$, $\langle v \rangle = 32$) and 13–14 CO_2 molecules solvating the cluster, moving to a much colder distribution ($0 \leqslant v \leqslant 17$, $\langle v \rangle = 3$) and 11–12 CO_2 molecules by 10 ps. The fit is quite good, except at energies $\leqslant 0.4$ eV in the spectra between 0.7 and 2.9 ps; this is discussed below.

The simulations indicate 4–5 CO_2 molecules have evaporated by 200 ps, and that the I_2^- chromophore is largely vibrationally relaxed, with $\langle v \rangle = 3$. This means nearly all the available energy from relaxation on the X state has been transferred to the various solvent vibrational and librational modes. However, comparison with the photofragmentation study by Vorsa,[35] in which the dominant product fragments are $I_2^-(CO_2)_{9,10}$, indicates that solvent evaporation is not complete by 200 ps. Thus, at 200 ps, the remaining excess energy is distributed among the solvent modes, and the time-scale for further solvent evaporation is likely to be described statistically. The incomplete evaporation by 200 ps is consistent with recent simulations by Faeder and Parson, who predict minimum time-scales of several hundred ps for complete evaporation.[36]

We next consider the interpretation of feature B. This feature is a distinct peak at 0.2 and 0.4 ps, but from 0.7 to 2.9 ps it appears more as a shoulder in the spectra around 0.4 eV. At 0.2 ps, it is reasonable to assign feature B to newly formed $I^-(CO_2)_n$ within the cluster; the shift from bare I^- is equivalent to solvation by 8–9 CO_2 molecules. This number does not reflect the number of CO_2 molecules in the cluster, only the average

Table 1 Average values of parameters used to fit the $I_2^-(CO_2)_{16}$ FPES spectra between 0.7 and 200 ps

time/ps	$\langle v \rangle^a$	$\langle E_{vib} \rangle^b$/eV	$\langle n \rangle^c$
0.7	40.5	0.482	14.5
1.0	40.5	0.482	14.5
1.6	32.1	0.396	13.5
2.9	17.5	0.231	13.5
4	7.3	0.104	11.7
6	4.8	0.071	11.5
10	3.1	0.049	11.5
200	3.1	0.049	11.5

[a] Average vibrational level. [b] Average vibrational energy. [c] Average number of CO_2 molecules.

number close enough to the I^- to interact with it. There are two possible interpretations to the subsequent evolution of this feature. One can consider this evolution as a steady decrease of intensity of feature B from 0.4 to 2.9 ps and attribute this decrease to depletion of solvated I^- *via* recombination on the X state to form vibrationally excited I_2^-. Alternatively, the change in appearance of feature B from a distinct peak at 0.4 ps to a shoulder at 0.7 ps can be interpreted as recombination on the A state, with the disappearance of the shoulder between 0.7 and 4 ps due to leakage out of the A state and onto the X state. According to this mechanism, which is depicted in the 'cartoon' in Fig. 8, recombination on both the X and A state occurs starting around 0.7 ps, but no population remains on the A state by 4.0 ps.

The second mechanism is more in line with Lineberger's experiments and Parson's simulations,[25] both of which suggest that recombination on the A state plays a role in the overall dynamics. In contrast to the photodissociation of $I_2^-(Ar)_{20}$, the stronger interactions with the CO_2 solvent molecules are likely to shorten the lifetime of this excited state significantly, consistent with disappearance of the shoulder by 4 ps. It would also be somewhat surprising for the solvated I^- to persist for several picoseconds, given that recombination in $I_2^-(Ar)_{20}$ occurs in 1 ps, and all other processes common to both clusters occur more rapidly in clusters with CO_2. We therefore favour the mechanism involving some short-lived recombination on the A state. However, to really distinguish the two mechanisms it is necessary to have a better understanding of the A state and how I_2^- molecules in that state interact with CO_2 solvent molecules.

Conclusions

Time-resolved photodissociation studies of $I_2^-(CO_2)_{n=4,16}$ clusters have been performed using femtosecond photoelectron spectroscopy (FPES). The $I_2^-(CO_2)_4$ spectra show that the I^- photofragment initially moves away from the cluster, but the attractive interaction between the I^- and CO_2 molecules is sufficiently strong that the I^- is prevented from escaping. Instead, from 0.2 to 0.5 ps, it is drawn toward the solvent molecules and complexes with several of them. This differs from the scenario for $I_2^-(Ar)_6$ photodissociation, in which the attraction between the I^- and Ar atoms is sufficiently weak that the anion solvent interaction decreases monotonically subsequent to photodissociation of the I_2^- chromophore. The FPES of $I_2^-(CO_2)_4$ for times greater than 0.7 ps appear to be from a distribution of $I^-(CO_2)_n$ clusters, with the $n = 2$ and 3 clusters present in approximately equal amounts as long as 200 ps after the dissociation pulse.

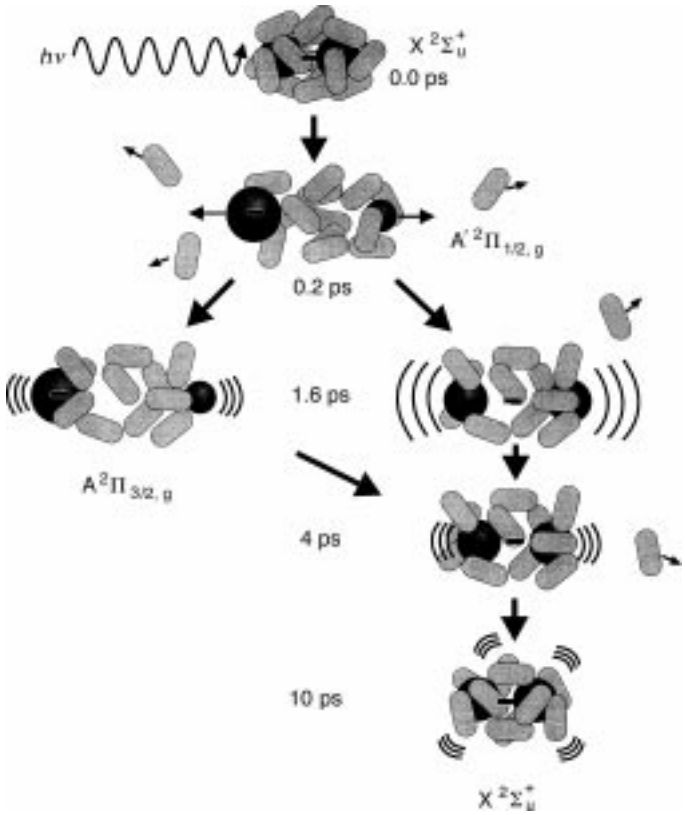

Fig. 8 'Cartoon' of $I_2^-(CO_2)_{16}$ cluster evaporation and recombination dynamics. Symbols are identical to those in Fig. 6.

Comparison with photofragment ion mass spectra taken several microseconds after dissociation indicates that solvent evaporation is incomplete at 200 ps.

In $I_2^-(CO_2)_{16}$ the FPES experiment allows us to follow a complex series of events that occurs subsequent to photodissociation of the I_2^- chromophore. Dissociation results in a partially solvated I^- chromophore which can be distinctly observed out to 0.4 ps. We interpret the spectra at longer times to indicate that recombination occurs on both the A and X states of I_2^-. Recombination on the A state is short-lived, and by 4 ps only the X state is populated. Starting at 0.7 ps, we can monitor the process of vibrational relaxation on the X state and the accompanying evaporation of solvent molecules. We find vibrational relaxation to be largely complete by 10 ps, but solvent evaporation is not complete even by 200 ps. The role of the A state is the most uncertain component of our interpretation and requires further experimental and theoretical investigation.

This work is supported by the National Science Foundation under Grant No. CHE-9710243 and the Defense University Research Instrumentation Program under Grant No. F49620-95-1-0078.

References

1 R. E. Smalley, L. Wharton and D. H. Levy, *J. Chem. Phys.*, 1978, **68**, 671.
2 R. J. Le Roy and J. S. Carley, *Adv. Chem. Phys.*, 1980, **42**, 353.

3 N. Halberstadt and K. C. Janda, *Dynamics of Polyatomic van der Waals Clusters*, Plenum, New York, 1990.
4 J. J. Breen, D. M. Willberg, M. Gutmann and A. H. Zewail, *J. Chem. Phys.*, 1990, **93**, 9180.
5 Q. L. Liu, J.-K. Wang and A. H. Zewail, *Nature* (*London*), 1993, **364**, 427.
6 A. W. Castleman, Jr. and K. H. Bowen, Jr., *J. Phys. Chem.*, 1996, **100**, 12911.
7 M. L. Alexander, N. E. Levinger, M. A. Johnson, D. Ray and W. C. Lineberger, *J. Chem. Phys.*, 1988, **88**, 6200.
8 J. M. Papanikolas, J. R. Gord, N. E. Levinger, D. Ray, V. Vorsa and W. C. Lineberger, *J. Phys. Chem.*, 1991, **95**, 8028.
9 J. M. Papanikolas, V. Vorsa, M. E. Nadal, P. J. Campagnola, J. R. Gord and W. C. Lineberger, *J. Chem. Phys.*, 1992, **97**, 7002.
10 J. M. Papanikolas, V. Vorsa, M. E. Nadal, P. J. Campagnola, H. K. Buchenau and W. C. Lineberger, *J. Chem. Phys.*, 1993, **99**, 8733.
11 D. Ray, N. E. Levinger, J. M. Papanikolas and W. C. Lineberger, *J. Chem. Phys.*, 1989, **91**, 6533.
12 A. M. Sanov and W. C. Lineberger, 1997, unpublished work.
13 V. Vorsa, P. J. Campagnola, S. Nandi, M. Larsson and W. C. Lineberger, *J. Chem. Phys.*, 1996, **105**, 2298.
14 V. Vorsa, S. Nandi, P. J. Campagnola, M. Larsson and W. C. Lineberger, *J. Chem. Phys.*, 1997, **106**, 1402.
15 B. J. Greenblatt, M. T. Zanni and D. M. Neumark, *Chem. Phys. Lett.*, 1996, **258**, 523.
16 B. J. Greenblatt, M. T. Zanni and D. M. Neumark, *Science*, 1997, **276**, 1675.
17 M. E. Nadal, P. D. Kleiber and W. C. Lineberber, *J. Chem. Phys.*, 1996, **105**, 504.
18 D. E. Smith and C. B. Harris, *J. Chem. Phys.*, 1987, **87**, 2709.
19 A. E. Johnson, N. E. Levinger and P. F. Barbara, *J. Phys. Chem.*, 1992, **96**, 7841.
20 P. K. Walhout, J. C. Alfano, K. A. M. Thakur and P. F. Barbara, *J. Phys. Chem.*, 1995, **99**, 7568.
21 L. Perera and F. G. Amar, *J. Chem. Phys.*, 1989, **90**, 7354.
22 V. S. Batista and D. F. Coker, *J. Chem. Phys.*, 1997, **106**, 7102.
23 J. M. Papanikolas, P. E. Maslen and R. Parson, *J. Chem. Phys.*, 1995, **102**, 2452.
24 J. Faeder and R. Parson, *J. Chem. Phys.*, 1998, in press.
25 N. Delaney, J. Faeder, P. E. Maslen and R. Parson, *J. Phys. Chem. A*, 1997, **101**, 8147.
26 W. C. Wiley and I. H. McLaren, *Rev. Sci. Instrum.*, 1955, **26**, 1150.
27 O. Cheshnovsky, S. H. Yang, C. L. Pettiette, M. J. Craycraft and R. E. Smalley, *Rev. Sci. Instrum.*, 1987, **58**, 2131.
28 L.-S. Wang, H.-S. Cheng and J. Fan, *J. Chem. Phys.*, 1995, **102**, 9480.
29 H. Handschuh, G. Gantefor and W. Eberhardt, *Rev. Sci. Instrum.*, 1995, **66**, 3838.
30 M. D. Davidson, B. Broers, H. G. Muller and H. B. van Linden van den Heuvell, *J. Phys. B*, 1992, **25**, 3093.
31 M. T. Zanni, T. R. Taylor, B. J. Greenblatt, B. Soep and D. M. Neumark, *J. Chem. Phys.*, 1997, **107**, 7613.
32 D. W. Arnold, S. E. Bradforth, E. H. Kim and D. M. Neumark, *J. Chem. Phys.*, 1995, **102**, 3510.
33 Y. Zhao, C. C. Arnold and D. M. Neumark, *J. Chem. Soc., Faraday Trans.*, 1993, **89**, 1449.
34 I. Yourshaw, Y. Zhao and D. M. Neumark, *J. Chem. Phys.*, 1996, **105**, 351.
35 V. Vorsa, PhD Thesis, University of Colorado, Boulder, 1996.
36 J. Faeder, N. Delaney and R. Parson, personal communication, 1997.
37 E. C. M. Chen and W. E. Wentworth, *J. Phys. Chem.*, 1985, **89**, 4099.
38 D. R. T. Appadoo, R. J. Leroy, P. F. Bernath, S. Gerstenkorn, P. Luc, J. Verges, J. Sinzelle, J. Chevillard and Y. Daignaux, *J. Chem. Phys.*, 1996, **104**, 903.
39 X. N. Zheng, S. L. Fei, M. C. Heaven and J. Tellinghuisen, *J. Chem. Phys.*, 1992, **96**, 4877.
40 J. W. Tromp and R. J. Le Roy, *J. Mol. Spectrosc.*, 1985, **109**, 352.
41 F. Martin, R. Bacis, S. Churassy and J. Verges, *J. Mol. Spectrosc.*, 1986, **116**, 71.

Paper 7/05890J; *Received* 12*th August*, 1997